MODEL-BASED SEGMENTATION TECHNIQUES FOR MULTI-FREQUENCY POLARIMETRIC SAR

P. Lombardo, M. Sciotti, T. Macrì Pellizzeri, M. Meloni

University of Rome "La Sapienza" – Via Eudossiana 18 - 00184 Rome, Italy.
Ph. +39-0644585412 Fax: +39-064873300 E-mail: lombardo@infocom.uniroma1.it

ABSTRACT

A new technique, named DPOL MUM, is proposed for the segmentation of multi-frequency polarimetric SAR images. By following a Maximum Likelihood approach, an optimal split-merge test is derived, which fully exploits the characteristic block-diagonal structure of the data covariance matrix. This test is demonstrated to yield a reduced fluctuation error than the extension of the polarimetric test to the multi-frequency case (POL MUM). Moreover, such test represents the basic step of a presently implemented region-growing segmentation technique. The performance comparison shows that the newly introduced technique outperforms the previous split-merge techniques in the segmentation of synthetic and real multi-frequency polarimetric SAR images of land areas.

1. INTRODUCTION

Many techniques have been proposed for optimal segmentation and terrain classification using SAR data, [1], and a large amount of data is presently available as collected by new SAR sensors, e.g. the fully-polarimetric ASAR onboard the ENVISAT spacecraft. It is well known that multi-frequency polarimetric SAR images carry appreciably more information on the observed scene than single-channel images. In particular, the reflectivity at the different frequencies and both the reflectivity and the phase relationships between the different polarimetric channels provide useful indications on the characteristics of the different observed objects, allowing a more accurate classification [2]. Many techniques for polarimetric SAR images are suited to pixel-by-pixel polarimetric classification, whereas it has been clearly demonstrated ([1,3]) that large performance improvement can be achieved by first segmenting the image into homogeneous regions, and then classifying the resulting global regions. It is therefore of interest to define optimal segmentation techniques for multi-frequency polarimetric SAR images. Moreover, the use of multi-frequency polarimetric SAR images yields a further improvement in the identification and classification of homogeneous regions with slightly different characteristics. An effective approach for segmenting polarimetric SAR data has been proposed in [3-4], and it can be easily extended to perform joint segmentation of any set of complex correlated SAR images, e.g. multi-band polarimetric images. However, the corresponding increase of dimensionality implies an increased level of uncertainty in the test, that is a potential source of performance degradation. However, it is usual to model the images acquired at different frequencies as uncorrelated. The exploitation of such model, that corresponds to a block diagonal covariance matrix, largely reduces the uncertainty in the segmentation test and can yield much better performance than the simple extension of the polarimetric segmentation scheme. Therefore, we derive an optimal segmentation technique that fully exploits such statistical model, and evaluate its performance both theoretically and on simulated data. The application to real SAR images shows the practical results obtained with the proposed technique.

2. MAXIMUM LIKELIHOOD POLARIMETRIC SEGMENTATION OF SAR DATA

The techniques proposed in [1,3-4] for segmenting speckled SAR images follow a generalised Maximum Likelihood (ML) criterion, based on the joint Probability Density Function (PDF) of the pixels in each homogeneous region. We adopt a multivariate Gaussian model to describe the statistical behaviour of the single-channel echoes, [1], and follow a similar approach. The joint PDF of the N pixels of a single region can be written as

$$p(\mathbf{x}) = \pi^{-MN} \left|R\right|^{-N} \exp\left[- Tr\left\{\mathbf{R}^{-1} \sum_{n=1}^{N} \mathbf{x}_n \mathbf{x}_n^{H}\right\}\right] \tag{1}$$

where the echoes received from the same resolution cell on the M polarimetric channels are arranged into the M dimensional vector, $\mathbf{x} = [x_1, \cdots, x_M]^T$, whereas $\mathbf{R}$ is the polarimetric complex covariance matrix and $\mathrm{Tr}\{\mathbf{A}\}$ and $|\mathbf{A}|$ stand for the trace and the determinant of the matrix $\mathbf{A}$ respectively. Eq. (1) also defines the likelihood of the N pixels belonging to a region with known covariance matrix $\mathbf{R}$. Since in general $\mathbf{R}$ is not known, we resort to the generalised likelihood by replacing the unknown covariance matrix with its ML estimate. Using such ML approach, a split-merge test can be derived. This is required to test whether two regions A and B, with N_A and N_B pixels respectively, belong to the same statistic (and thus must be merged): hypothesis H_0, or do not belong to the same statistic (and thus must be

split): hypothesis H_1. Naming as $\mathbf{R}^{(A)}$ and $\mathbf{R}^{(B)}$ the covariance matrices of the two different regions in hypothesis H_1, and as $\mathbf{R}^{(0)}$ the common covariance matrix in the hypothesis H_0, the generalised likelihood test for the two hypotheses yields

$$\Lambda_M = \Lambda_M(N_A, N_B) = C^M \cdot \left|\boldsymbol{\Sigma}^{(A)}\right|^{N_A} \left|\boldsymbol{\Sigma}^{(B)}\right|^{N_B} \left|\boldsymbol{\Sigma}\right|^{-N} > \lambda \tag{2}$$

where λ is an appropriate threshold and the matrices are given by

$$\Sigma^{(A)} = \sum_{n=1}^{N_A} \mathbf{x}_n^{(A)} \mathbf{x}_n^{(A)H}; \quad \Sigma^{(B)} = \sum_{n=1}^{N_B} \mathbf{x}_n^{(B)} \mathbf{x}_n^{(B)H}; \quad \Sigma = \sum_{n=1}^{N} \mathbf{x}_n \mathbf{x}_n^H = \sum_{n=1}^{N_A} \mathbf{x}_n^{(A)} \mathbf{x}_n^{(A)H} + \sum_{n=1}^{N_B} \mathbf{x}_n^{(B)} \mathbf{x}_n^{(B)H} = \Sigma^{(A)} + \Sigma^{(B)} \tag{3}$$

corresponding to the scaled sample correlation matrix in the regions A, B, and A+B. Moreover, we have set $N=N_A+N_B$ and the constant C is given by $C = C(N_A, N_B) = N^N / (N_A^{N_A} N_B^{N_B})$. The split-merge test in Eq. (2) is the basic step of the region-growing segmentation technique which was described in [4] as a possible alternative to the POLSEGANN technique that was used therein. This approach, named Polarimetric Merge-Using-Moments (POL MUM), has presently been implemented into an effective segmentation routine and directly generalised for the multi-frequency polarimetric case, by simply increasing the dimensionality of the input vector **x** and replacing the number of polarimetric channels M with the sum of all available multi-frequency polarimetric channels, $M_1+M_2=M$. The POL MUM routine makes no assumption on the structure of the covariance matrix and is particularly suited for single-frequency polarimetric images, where the echoes collected at different channels show high degrees of statistical correlation. When dealing with multi-frequency data, a specific structure for the covariance matrix should be considered in the segmentation algorithm, in order to reduce the adaptivity losses introduced by the matrix local estimation. In particular, we consider the case of a block diagonal structure for the covariance matrix, i.e.

$$\mathbf{R} = \begin{bmatrix} \mathbf{R}_1 & \mathbf{0} \\ \mathbf{0} & \mathbf{R}_2 \end{bmatrix} \tag{4}$$

where $\mathbf{R}_1$ and $\mathbf{R}_2$ are respectively M_1-dimensional and M_2-dimensional unknown polarimetric covariance matrices, with $M_1+M_2=M$. This is usually the case for multi-frequency polarimetric SAR data, where the data at the different frequencies show a very low correlation, due to the different combination of the speckle phase contribution and, possibly, to the different scattering mechanism involved. By splitting the data vector for the single pixel as $\mathbf{x} = [\mathbf{x}_1^T, \mathbf{x}_2^T]^T = [x_{1,1}, \cdots, x_{1,M_1}, x_{2,1}, \cdots, x_{2,M_2}]^T$, the PDF of N pixels can be easily rewritten as the product of the two marginal PDFs and this can be exploited to derive a model-based segmentation technique for multi-frequency data. Specifically, under this assumption the split-merge test obtained using the generalised likelihood test for the two hypotheses yields

$$\Phi_M = \Phi_M(N_A, N_B) = C^M \cdot \frac{\left|\boldsymbol{\Sigma}_1^{(A)}\right|^{N_A} \left|\boldsymbol{\Sigma}_1^{(B)}\right|^{N_B}}{\left|\boldsymbol{\Sigma}_1\right|^{N}} \cdot \frac{\left|\boldsymbol{\Sigma}_2^{(A)}\right|^{N_A} \left|\boldsymbol{\Sigma}_2^{(B)}\right|^{N_B}}{\left|\boldsymbol{\Sigma}_2\right|^{N}} > \lambda \tag{5}$$

where the matrices have been defined consistently with Eq. (3) and we have

$$\Sigma_1 = \Sigma_1^{(A)} + \Sigma_1^{(B)} \qquad \Sigma_2 = \Sigma_2^{(A)} + \Sigma_2^{(B)} \tag{6}$$

The split-merge test in Eq. (5) is the basic step of a split-merge approach, named Diagonal POLarimetric Merge-Using-Moments test (DPOL MUM), that has presently been implemented into an effective segmentation routine. The algorithm iteratively tests adjacent segments for homogeneity and merges the mostly homogeneous set of adjacent segments, following a similar approach as the one described in [4].

3. COMPARATIVE PERFORMANCE ANALYSIS

To fully compare the performance of the different split-merge tests, we define the probability of false alarm (P_{fa}) as the probability of erroneously splitting two homogeneous regions, and the probability of detection (P_d) as the probability of correctly splitting two adjacent regions that have a multi-frequency polarimetric difference. An analytic expression of the P_{fa} is required as a function of the number of pixels of the two regions under test, and of the threshold λ. Unfortunately the PDF of the likelihood ratio under hypothesis H_0 ($\mathbf{R}^{(A)}=\mathbf{R}^{(B)}=\mathbf{R}^{(0)}$) is unknown; thus, we derived in [5] an approximate expression for the PDF and consequently the P_{fa}. By defining the scaling parameter

$$\rho_M = 1 - \frac{M^2 - 1}{6M} \left(\frac{1}{N_A} + \frac{1}{N_B} - \frac{1}{N} \right) \tag{7}$$

the following expression for the P_{fa} is obtained:

$$P_{fa} = 1 - \sum_{k=1}^{M_1^2/2} A_k \, \gamma(k, -\rho_{M_1} \ln \lambda) - \sum_{j=1}^{M_2^2/2} B_j \, \gamma(j, -\rho_{M_1} \ln \lambda) \quad (8)$$

where A_k and B_j are coefficients as obtained from the expansion of the Laplace transform of the derived PDF (see [5]). To validate the approximate expression in Eq. (8), a complete simulated analysis was carried out. The results show a good fit between the predicted and simulated curves of P_{fa}, thus allowing the use of the approximated performance in the segmentation routine in order to control the fusion of adjacent regions and the stopping criterion.

In contrast, an expression of the discrimination capability of the split-merge tests is hardly achievable, and thus we resort to Monte Carlo simulation. Specifically, we derive the ROCs (Receiver Operating Characteristics) for different values of $\mathbf{R}_1^{(A)}$, $\mathbf{R}_1^{(B)}$ and $\mathbf{R}_2^{(A)}$, $\mathbf{R}_2^{(B)}$. We consider four cases which are representative of possible conditions of two regions that have the same polarimetric behaviour on the first frequency and a polarimetric difference on the second:

- case (a) $$\mathbf{R}_1^{(A)} = \mathbf{R}_1^{(B)} = \mathbf{R}_2^{(A)} = \begin{bmatrix} 1 & 0.3 \\ 0.3 & 1 \end{bmatrix}; \; \mathbf{R}_2^{(B)} = \begin{bmatrix} 1 & 0.85 \\ 0.85 & 1 \end{bmatrix}; \quad (9)$$

- case (b) $$\mathbf{R}_1^{(A)} = \mathbf{R}_1^{(B)} = \mathbf{R}_2^{(A)} = \begin{bmatrix} 1 & 0 \\ 0 & 1 \end{bmatrix}; \; \mathbf{R}_2^{(B)} = \begin{bmatrix} 1 & 0.9 \\ 0.9 & 1 \end{bmatrix}; \quad (10)$$

- case (c) $$\mathbf{R}_1^{(A)} = \mathbf{R}_1^{(B)} = \mathbf{R}_2^{(A)} = \begin{bmatrix} 1 & 0.75 \\ 0.75 & 1 \end{bmatrix}; \; \mathbf{R}_2^{(B)} = \begin{bmatrix} 5 & 0.85 \\ 0.85 & 5 \end{bmatrix}; \quad (11)$$

- case (d) $$\mathbf{R}_1^{(A)} = \mathbf{R}_1^{(B)} = \mathbf{R}_2^{(A)} = \begin{bmatrix} 1 & 0.75 \\ 0.75 & 1 \end{bmatrix}; \; \mathbf{R}_2^{(B)} = \begin{bmatrix} 1.5 & 0.85 \\ 0.85 & 1.5 \end{bmatrix}; \quad (12)$$

Figs. 1(a)-(d) show the ROC curves as obtained for POL MUM and DPOL MUM tests, when applied to two adjacent regions of N=16 pixels. The performance of the Multi-Temporal Merge-Using-Moments test (MT MUM) is also reported for comparison, [6], as this latter test has been derived following the approach of Eq. (2) and assuming $\mathbf{R}^{(A)}$ and $\mathbf{R}^{(B)}$ fully diagonal. As expected, the MT MUM does not make use of the correlation property of the different channels, so that the Polarimetric MUM-based tests always outperform MT MUM as they fully exploit the information contained in the polarimetric covariance matrix. It is evident that:

(i) the performance improvement is large when the mean reflectivity of region B at the second frequency is unchanged, while only the correlation between the two polarimetric channels changes, i.e. cases (a) and (b);
(ii) DPOL MUM always outperforms POL MUM;
(iii) a strong reflectivity change is well detected by all tests, case (c), and DPOL MUM still performs the best;
(iv) in the worst case, namely the case of presence of a small reflectivity change together with only a small variation in the correlation coefficient, case (d), the three tests show similar performance.

Thus, a neat theoretical improvement is available when properly exploiting the considered model with DPOL MUM. This can be explained as follows. The DPOL MUM algorithm requires the estimation of the M_1- and M_2-dimensional covariance matrices on the N-pixel region, whereas the application of POL MUM requires the estimate of an M= M_1+M_2- dimensional covariance matrix on the same N-pixels region. In consequence, the newly proposed, model-based test yields better discrimination performance, as being affected by a lower estimation error. This improvement is available when the actual covariance matrix of the data is really block diagonal, which is certainly the case for the considered multi-frequency data.

4. SEGMENTATION OF SYNTHETIC AND REAL SAR DATA

Figs. 2(a-d) show the results obtained by applying the MT MUM, POL MUM and DPOL MUM algorithms to a set of synthetic images. To emulate the case of six channels of dual frequency polarimetric SAR data, we consider a set of six images (M=6), characterised by a block diagonal covariance matrix. The size of each block is M_1=M_2=3, and for simplicity of simulation the two blocks are considered identical. Fig. 2(a) shows the original pattern comprised of 7 regions with different polarimetric covariance matrix, whereas Fig. 2(b) reports the intensity image for one of the simulated channels. From the analysis of the different covariance matrices, the following observations apply: (i) the average intensity of the three channels is the same for all classes, and the intensity of the second channel is definitely higher than the intensities of the other two for all the classes; (ii) the covariance matrices of classes 1, 3, and 4 have the same determinant (0.1), while the determinant of the covariance matrix of class 6 is equal to 0.1005; (iii) classes 4 and 7 show very similar intensities for the three channels, and thus can be confused if relying only on the intensity values.

To compare the segmentation performance of the three considered algorithms, we generate 10 independent sets of synthetic images, and we perform a segmentation with all three algorithms on each set. We choose the value of P_{fa} that maximises the probability of correct classification against the test pattern. Then, to provide a quantitative performance measure for the different segmentation schemes, we apply the same classifier to the regions identified with the different

techniques. In particular, we use a ML supervised classifier, based on the statistical model in Eq. (1), assuming that the polarimetric characteristics of the seven classes $c = 1,\ldots, 7$ are known (i.e. their covariance matrix $\mathbf{R_c}$ is known). Figs. 2(c)-(f) show the results for one of the considered sets. In particular, Fig. 2(c) shows the classification output for the MT MUM, while Fig. 2(d) shows the classification pattern as obtained with POL MUM, and Figs. 2(e)-(f) report the segmentation and classification output for the newly conceived DPOL MUM technique. It is to be noticed that:

- the big circular region in the upper left part of the image is not clearly identified by MT MUM. Moreover, some homogeneous regions have been over-segmented by MT MUM, and some others completely disappear, as in particular the diagonal strip from the upper right to the lower left part of the image. This is consistent with our expectations, since the strip belongs to class 4, while the surrounding region belongs to class 7. As previously noticed, the two classes have very similar intensities, thus they are merged. On the contrary, when using the full covariance matrix to perform segmentation (namely when using POL MUM and DPOL MUM) the differences between the two regions are more evident and thus they are not merged.
- Both POL MUM and DPOL MUM exploit the polarimetric data properties, and consequently outperform MT MUM. However, POL MUM still over-segments some regions and the region borders are less smoothed than those obtained with DPOL MUM. This is due to the initial decomposition of the input images in square regions of 3x3 pixels (2x2 for DPOL MUM), that is required for the estimation of all the elements of the 6x6 covariance matrix.
- A non negligible percentage of the pixels of class 3 is misclassified by all three techniques. This is a consequence of the limited number of pixels belonging to this class, that causes the classification performance to be very sensitive to small variations in the shape of the region borders.
- The percentage of correctly classified pixels operating with DPOL MUM is generally higher than with POL MUM. The improvement is more evident for classes 2, 5, and 7, for which such percentage raises respectively from 90.5% to 99.6% (class 2), from 93.1% to 98.2% (class 5), and from 92.7% to 98.2% (class 7). This is a consequence of a more accurate identification of the region borders, and it is more evident for these classes since their borders are not vertical or horizontal lines, thus they are more difficult to be identified correctly by the segmentation algorithm.

Finally, to provide a global measure of the classification accuracy achievable with the different techniques, we evaluate the average probability of correct classification (P_{cor}) for the whole image. The above comments of the simulated analysis are largely confirmed. In particular, the use of the polarimetric information largely increases the accuracy in the identification of the different regions (P_{cor} raises from 72.3% for MT MUM to more than 92% for the polarimetric routines). Moreover, the exploitation of the a priori information for the structure of the covariance matrix provides a further increase in the identification accuracy, yielding a P_{cor} of 96%.

To show the effectiveness of the proposed segmentation technique we consider a set of SIR-C dual-frequency polarimetric images of the town of Pavia, in Northern Italy. Fig. 3(a) shows the C-band HH high-resolution image. For simplicity, in our analysis, we only consider the two like-polarised channels. A partial knowledge of the ground truth is available for the considered data set, composed of three different classes: (i) water, (ii) agricultural area, and (iii) built up area. The whole ground truth is split into a training set and a test set, respectively used to estimate the covariance matrix of the different classes and to evaluate the classification results. The test set is reported in Fig. 3(b). We apply the different segmentation routines to the considered data, for different values of the P_{fa} and of the size of the initial tessellation of the image. We then apply the ML classifier to each one of the segmented images, and select the values of the parameters which yield the highest average probability of correct classification. The resulting classified images are shown in Fig. 3 (c,d,f), respectively for MT MUM, POL MUM, and DPOL MUM, while Fig. 3(e) shows the segmentation output for DPOL MUM. It is apparent that DPOL MUM tends to identify a higher number of homogeneous regions, and it tends to identify more accurately the borders. This is a consequence of (i) the increased amount of used information with respect to MT MUM, and (ii) the lower level of noise in the estimation of the covariance matrix with respect to POL MUM. Unfortunately, the higher polarimetric sensitivity also yields isolated pixels that are not merged as expected; however, this does not degrade globally the classification performance. Finally, as expected, the higher accuracy provided by DPOL MUM in the identification of the borders of the homogeneous segments results in an increased accuracy in the classification (P_{cor} raises from 80.6% for MT MUM and 80.7% for POL MUM to 82.9% for DPOL MUM), showing the effectiveness of the novel algorithm for application to real data.

7. CONCLUSIONS

An effective technique, DPOL MUM, has been proposed for the segmentation of multi-frequency polarimetric SAR images, that exploits the characteristic block diagonal structure of their covariance matrix. This technique is based on the model based split-merge test, that has a reduced fluctuation error than the straight extension of the polarimetric test (POL MUM). An approximate analytic expression for the P_{fa} of this test has been derived in closed form to be used inside the algorithm to control the fusion of adjacent regions and the stopping criterion. A full Monte Carlo simulation is used to demonstrate that DPOLMUM yields better performance than both previous POL MUM and MT MUM

segmenters. Similarly an ML classification, performed after segmentation of both a set of simulated images and real SAR data, showed that segmenting with DPOL MUM yields a higher probability of correct classification than segmenting with both POL MUM and MT MUM. This demonstrates the effectiveness of the proposed model-based technique for the practical application over multi-frequency polarimetric images of land areas.

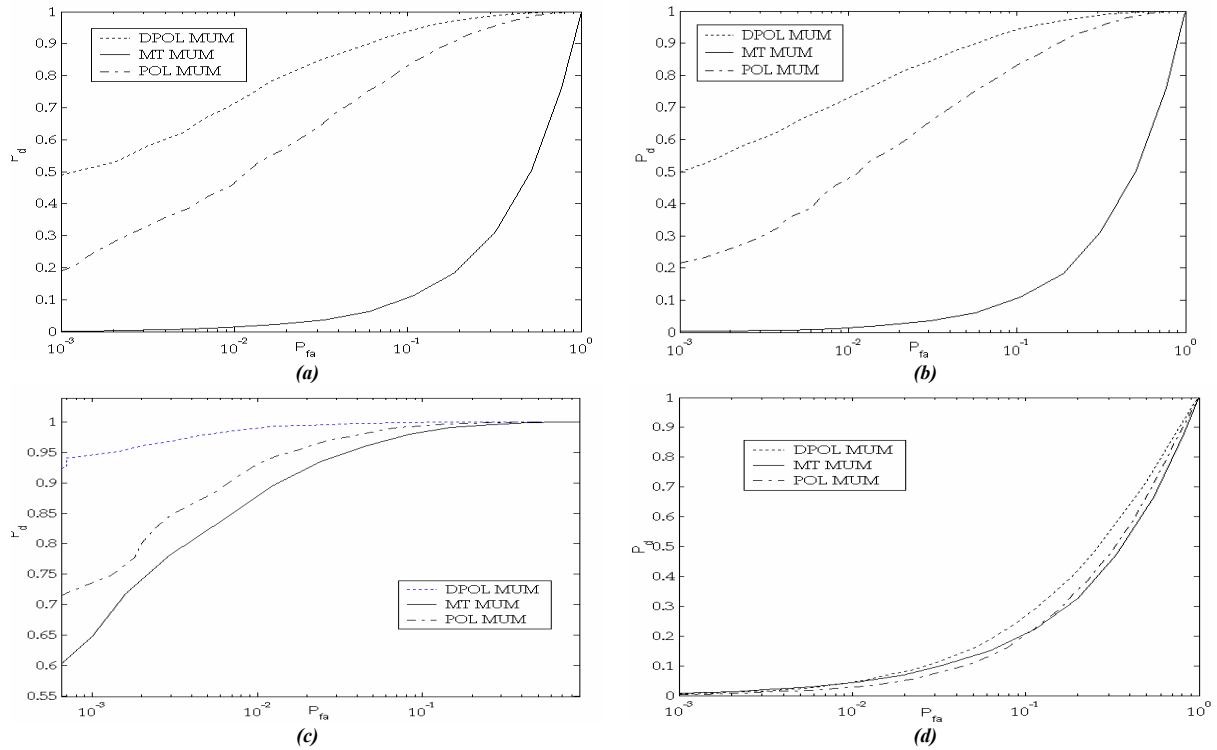

Fig. 1 (a)-(d) – Simulated ROCs of the split-merge tests for N_A=N_B=8 and $\mathbf{R_1}^{(A)}$, $\mathbf{R_1}^{(B)}$, $\mathbf{R_2}^{(A)}$, $\mathbf{R_2}^{(B)}$ given respectively in Eqs (9-12).

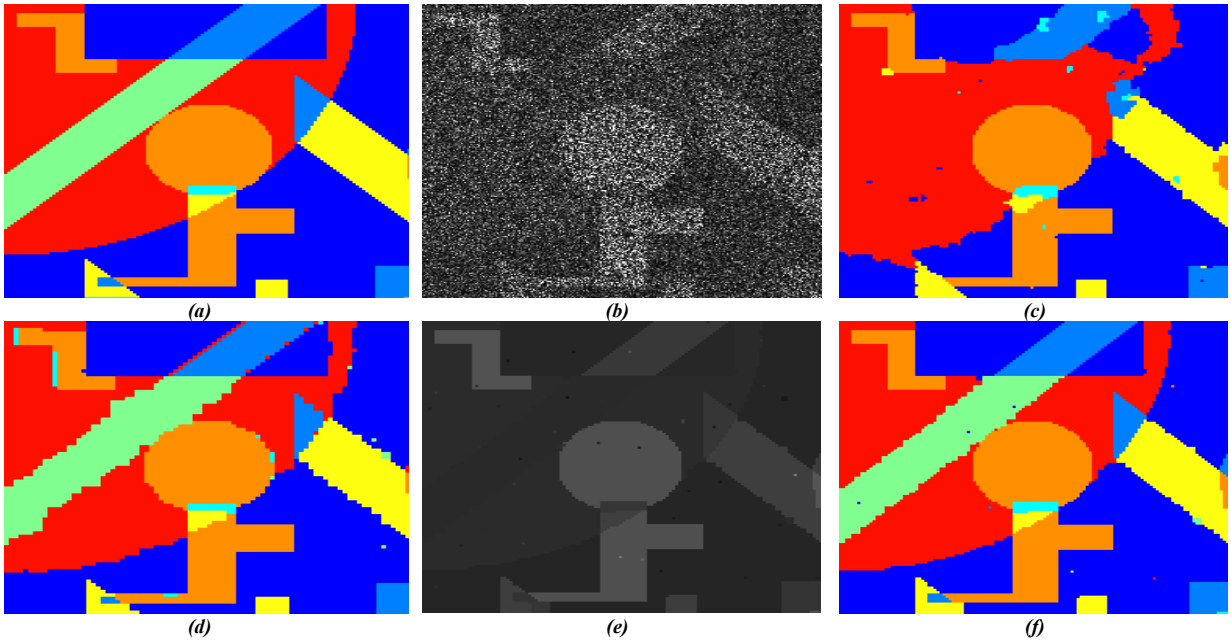

Fig. 2 (a)-(f) – Synthetic test images: (a) original pattern, (b) intensity image, (c) MT MUM classification output, (d) POL MUM classification output, (e) DPOL MUM segmented image, (f) DPOL MUM classification output.

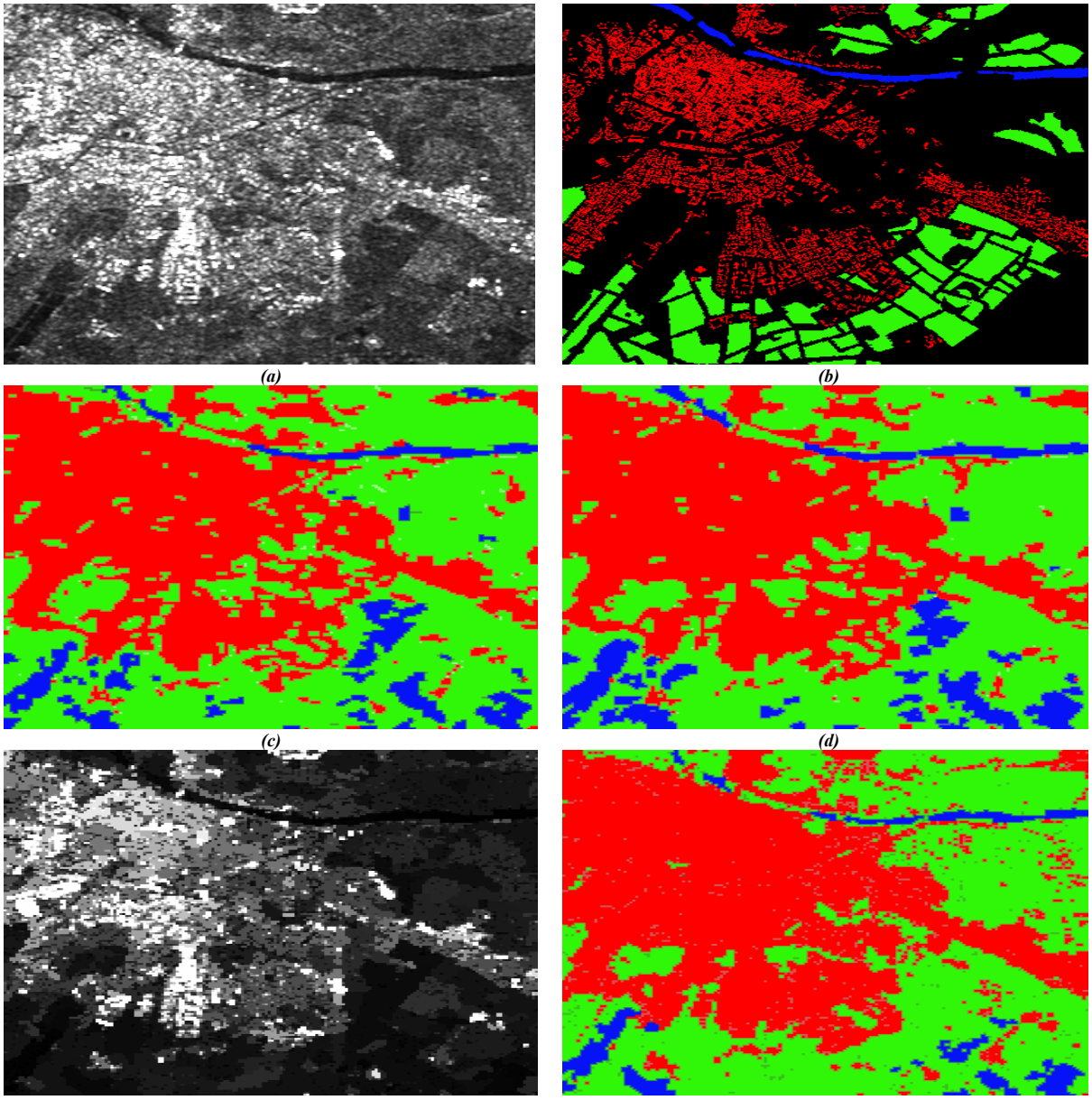

Fig. 3 (a)-(f) – SIR-C SAR test images: (a) C-band HH image, (b) test set, (c) MT MUM classification output, (d) POL MUM classification output, (e) DPOL MUM segmented image, (f) DPOL MUM classification output. Blue: water (class 1), green: agricultural areas (class 2), red: built-up areas (class 3).

8. REFERENCES

[1] C.J. Oliver, and S. Quegan, "*Understanding SAR images*", Artech House, NY, 1998.

[2] J.J. Van Zyl, H.A. Zebker, C. Elachi, "*Imaging radar polarization signatures: Theory and observations*", Radio Science, Vol. 22, 1987, pp. 529-543.

[3] P. Lombardo, C.J. Oliver, "*Optimal Classification of Polarimetric SAR images Using Segmentation",* IEEE Radar Conference 2002, Long Beach (CA), April 2002.

[4] P. Lombardo, C.J. Oliver, "Optimal *Polarimetric Segmentation for the Classification of Agricultural Areas*", EUSAR 2002, Koeln, Germany, June 2002.

[5] P. Lombardo, M. Sciotti, T. Macrì Pellizzeri, "*Optimum Model-based Segmentation Techniques for Multi-frequency Polarimetric SAR images of Urban Areas*", INFOCOM Tech. Report no. 005/05/02, December 2002.

[6] C.J. Oliver, I. McConnell, D.G. Corr, "*Multi-temporal change detection for SAR imagery*", Europto Conf. On SAR image analysis, modelling and techniques IV, Florence, Italy, SPIE Proc. 3869, 1999.